The effect of air-formed oxide film on copper corrosion during the initial phase of final deposition of nuclear waste

Jari Aromaa*, Ha Linh Vu and Mari Lundström

Aalto University, School of Chemical Engineering, P.O. Box 16200, 00075 Aalto, Espoo, Finland.

ABSTRACT

Spent nuclear fuel from the Finnish nuclear power plants is disposed in bedrock encapsulated in copper canisters. The canister wall thickness is nominally 50 mm, and the design lifetime is 100 000 years. The allowed corrosion rates are very low, and it is assumed that the most corrosive oxic period will last only some years in the beginning. In this paper we have studied the effect of initial oxide film on the corrosion rate, as the oxide films can catalyze cathodic reduction of oxygen and thus increase copper corrosion rate. The research was done by monitoring corrosion rates using linear polarization resistance (LPR) and comparing the corrosion rates of oxidized and non-oxidized specimens. Test environments were synthetic ground water and bentonite clay pore water under air purging and nitrogen purging at temperatures 20-80°C. The measured corrosion rates varied from less than one to almost 40 μm a^{-1}. Comparison of the environmental variables indicated that the corrosion rates in pH = 10 pore water were 60-70% lower than in pH = 8 ground water. The effect of dissolved oxygen was low. The activation energy calculations showed that corrosion was controlled by charge transfer and in some cases corrosion was under mixed control. The comparisons to determine the effect of oxide films were done using power law modelling, box-and-whisker plots, and statistical t-tests. The analyses showed that the oxide film has in most cases no effect on corrosion. Only in air-purged ground water at elevated temperatures the oxide film increased corrosion.

KEYWORDS: copper, corrosion, canister, nuclear waste, lifetime prediction.

INTRODUCTION

The Finnish plan for final deposition of nuclear waste is based on the KBS-3 concept. The spent fuel is encapsulated in gas-tight, corrosion resistant and load-bearing canisters. The spent fuel assemblies are loaded in cast iron load-bearing inserts, and these inserts are placed into copper canisters. The canisters are disposed in crystalline bedrock at a depth sufficient to isolate the encapsulated spent fuel from the surface environment, about 400 to 700 meters deep. In the deposition holes the canisters are surrounded by a compacted bentonite clay buffer that prevents the flow of water and protects them. Finally, the cavities in the rock that are required for the deposition of canisters are backfilled and closed. The goal of the long-term containment is that the safety functions shall effectively prevent release of disposed radioactive materials into the bedrock for at least several thousands of years [1, 2].

In this work we have studied the corrosion of copper canister material in simulated ground water and bentonite clay pore water using electrochemical monitoring with linear polarization method. Our study focuses on the effect of air-developed oxide film on general corrosion in the initial warm and oxic phase. After assembly the loaded spent fuel will cause increase in canister

*Corresponding author: jari.aromaa@aalto.fi

temperature. The surface temperature is less than 50ºC in freely circulating air, but close to 100ºC when in a radiation shield or in the deposition hole with unsaturated bentonite buffer and air space between canister and buffer [3, 4]. Before and after assembly the canisters are stored indoors before transport to underground temporary storage. The time from assembly to deposition can be up to a few months, and most of it is in underground storage [3, 5]. Before emplacement the copper canister will develop an oxide layer. The thickness of the oxide layer before deposition has been estimated as few tens or few hundreds of nanometres [4].

In the encapsulation plant and underground facility, the canisters may be subject to atmospheric corrosion if the relative humidity is sufficiently high. After emplacement of the canisters there will be a period of unsaturated conditions in the compacted bentonite, until the near-field environment (a few meters from the canister) saturates with incoming ground water. The corrosive environment around the canister will be a combination of initial bentonite pore water and saturating ground water. The nature of near-field environment will evolve with time as the repository environment gradually returns to its pre-excavation state as the heat dissipates, oxidants are consumed, and other redox processes take place [6]. After being positioned, the outer surface temperature of the canisters would be limited to a maximum value of 100°C. When the canister cools down and the trapped atmospheric oxygen is used up, the repository environment will become cool and anoxic. The corrosion processes will slow down and change from possibly localized to uniform corrosion. The consumption of trapped oxygen by reactions with the copper canister and microbes and minerals in the surrounding clay and backfill materials has been calculated to take tens or even hundreds of years [4].

King and Kolář divided the repository environment after final deposition into six periods from the initial oxic condition to the anaerobic state in long term [6]. The first period is considered the most corrosive with corrosion rates in the order of 10 μm a^{-1} due to high temperature, oxic environment and oxidizing conditions.

Chlorides and entrapped oxygen are the major contributors to copper corrosion at this stage. The first period will last from less than a year to some years. In the second stage, the container surface is too warm and dry for corrosion to occur. The cathodic reduction of oxygen has stopped by this point because the initial trapped oxygen has been consumed. The second stage may last up to hundred years after which corrosion starts again as the canister surface becomes re-wetted from water entering through the bentonite blocks. In the third stage after re-wetting oxic corrosion continues until all Cu^{2+} in the system is consumed. After that, no corrosion takes place until HS^{-} from the environment reaches the canister surface. The beginning of the sulfidic corrosion phase can take tens of thousands of years. Corrosion rates in the initial oxic period are in the order of 10 μm a^{-1} and only last for maximum some years. When the canister surface gets re-wetted, aerobic corrosion due to Cu^{2+} starts, but the corrosion rates are in the order of 0.1 μm a^{-1} decreasing to less than 1 nm a^{-1}. The corrosion rates in the final sulfidic corrosion phase are only in the order of 0.001 nm a^{-1} [6].

As most of the corrosion is expected to happen in the very first years of the final disposal, we have focused on general corrosion that may be affected by the initial oxide films. The air-formed oxide film can affect corrosion in a similar way as the oxide films formed during corrosion consisting of CuO and Cu_2O. Oxygen reduction on copper is inhibited by metal oxidation into the $Cu/Cu_2O/CuO$ duplex layer [7]. On copper surface the Cu(I) species are more catalytic to oxygen reduction than Cu(0), i.e. metallic copper [8]. The oxidation of Cu_2O by oxygen to CuO can inhibit oxygen reduction. On the other hand, Cu_2O can increase the total cathodic reaction rate by its own reduction, and this could result in slightly faster corrosion [9]. Based on mixed potential theory if the rate of oxygen reduction reaction increases, then the consumption of electrons will increase and that will increase copper corrosion rate. The reaction of cuprous chloride species with oxygen can result in cupric species and they can also act as oxidants [10].

The passivation of copper depends mainly on the pH of the environment. The concentration and

speciation of dissolved copper depends on the nature of the solid copper compounds, pH, chloride concentration, and temperature. The oxides Cu_2O and CuO are the thermodynamically favoured solids in alkaline solutions. According to [11] there is a minimum solubility of copper at pH 9-12. At pH 8-8.5 the reaction product layer is $CuCl/Cu_2O/CuO$ changing to $Cu_2O/CuO/Cu(OH)_2$ at pH 10-10.5. With increasing pH, the shift from passive to active state happens at higher chloride concentration, and the passivation potential is insensitive to chloride concentrations 0.1-1.0 mol dm^{-3}.

The expected trends or hypotheses for our research were:

- Corrosion rate in air-purged water is higher than in nitrogen-purged water. This due to corrosion being controlled by mass transfer of the main oxidant, that is dissolved oxygen.

- Corrosion rate is lower in high pH pore water than in near neutral ground water. This is due to stronger passivation in high pH water.

- Corrosion rate increases with increasing temperature. This is due to the increase of the charge transfer rate as indicated by the Arrhenius law.

- The oxide film can catalyse oxygen reduction leading to higher corrosion rate.

There are factors that can make the above-mentioned hypotheses more difficult to interpret, including:

- Solubility of oxygen is higher in pore water than in ground water due to lower concentration of total dissolved solids.

- Solubility of oxygen decreases with increasing temperature decreasing the cathodic reduction rate which in turn will decrease the rate of the anodic copper dissolution reaction.

- With time a sample can show passivation and depassivation and the corrosion rate does not show a clear trend with time.

MATERIALS AND METHODS

The test material was oxygen-free high-conductivity copper from Goodfellow Cambridge Ltd. The copper is described for example in standard SFS-EN 12165 "Copper and copper alloys. Wrought and unwrought forging stock". The minimum Cu+Ag is 99.95% with Ag maximum 0.015%. Bismuth and lead levels are typical for grade A copper cathodes, 0.0005% and 0.005% respectively. The oxygen content shall be so low that the material conforms to the hydrogen embrittlement requirements of EN 1976, typically max. 10 ppm. The copper canister construction material is same, but some 40-60 ppm phosphorus is alloyed. This should not to our knowledge affect oxidation or corrosion behaviour.

For electrochemical tests the samples were cut from 9.5 mm diameter rod and mounted in Struers metallographic sample epoxy. The samples were approximately 5 mm thick with a copper wire soldered in the back. The samples were prepared by water grinding and the finest silicon carbide grinding paper used had 500 grit particle size. Before the experiments all the samples were first degreased by ethanol and then immersed in 10 wt-% citric acid for 3 minutes at room temperature. Immersion was repeated 3 times and after each immersion the sample was rinsed with Millipore water and after last immersion with water and ethanol. After the last rinse the samples were dried with hot air. The oxidation of the samples was done in a drying oven (Pol-Eko SLW 53 Smart, Pol-Eko Aparatura, Wodzisław Śląski, Poland). Oxidation treatment lasted for 7 days at 100°C.

In electrochemical measurements an Autolab 31 potentiostat (Metrohm Autolab B. V., Utrecht, The Netherlands) with Nova 2.1 software (Metrohm Autolab B. V., Utrecht, The Netherlands) was used. In every test there were two oxidized and two non-oxidized samples immersed in the vessel, and three successive measurements were done for every sample. Every measurement point in linear polarization resistance (LPR) monitoring is thus average of six individual measurements. The LPR tests were performed from -30 mV to +30 mV vs. OCP using scan rate 1 mV s^{-1}. Corrosion current densities were determined using the curve fit application of the measurement software. The length of the LPR monitoring tests was up to 3 weeks. The reference electrode was Radiometer REF201 Red Rod Ag/AgCl electrode, and all potentials are reported versus saturated Ag/AgCl.

The groundwater recipe was based on the groundwater analyses of the Olkiluoto final deposition site [12] and pore water recipe based on the analysis given in [13]. The water compositions are shown in Table 1. LPR measurements were done at temperatures 20°C, 40°C, 60°C, and 80°C. The water-jacketed reactor volume was 1 litre, and dissolved oxygen level was controlled by using air or nitrogen purging at 0.25 dm^3 min^{-1}. The concentration of dissolved oxygen in air-purged waters was 6-7 ppm and in nitrogen-purged waters approximately 1 ppm.

RESULTS AND DISCUSSION

The corrosion rates measured in the linear polarization measurements showed in some cases a decreasing trend with time whereas in other cases no trend was seen. A challenge in analyzing the results and corrosion rates was the very low measured current. The measured corrosion current densities were usually in the order of 10^{-8} to 10^{-6} A cm^{-2} that correspond to approximately 0.1-10 μm a^{-1}.

Figure 1 shows examples of LPR measurements at the beginning of the test and at the end when the sample has passivated. The measurement shown in Figure 1 was done in pore water with air purging at T = 40°C. The initial currents of non-oxidized sample are higher than those of the oxidized sample, but with time they become almost the same. Figure 2 shows examples of the changes in the open circuit potential during the test. Generally, the variation in corrosion potential was tens of millivolts even after two weeks. As the gas purging and temperature was kept constant during the test the variation is a result of evolution of corrosion product layers.

The aim of this study was to determine whether an air-formed oxide film can increase the general or uniform corrosion rate of copper. The analysis was therefore based on comparisons of corrosion rates of oxidized and non-oxidized samples in the

Table 1. Composition of the test waters.

Component	Ground water (GW), mg/l	Pore water (PW), mg/l
Na	3610	1000
Cl	5340	80
SO$_4$	582	1300
Ca	279	4
Mg	102	4
K	87.5	12
Br	42	
HCO$_3$	13.7	960
Sr	7.71	
Si	6.25	
B	1.38	
F	0.74	
Mn	0.168	
pH	7.9	10
TDS	10070	3360
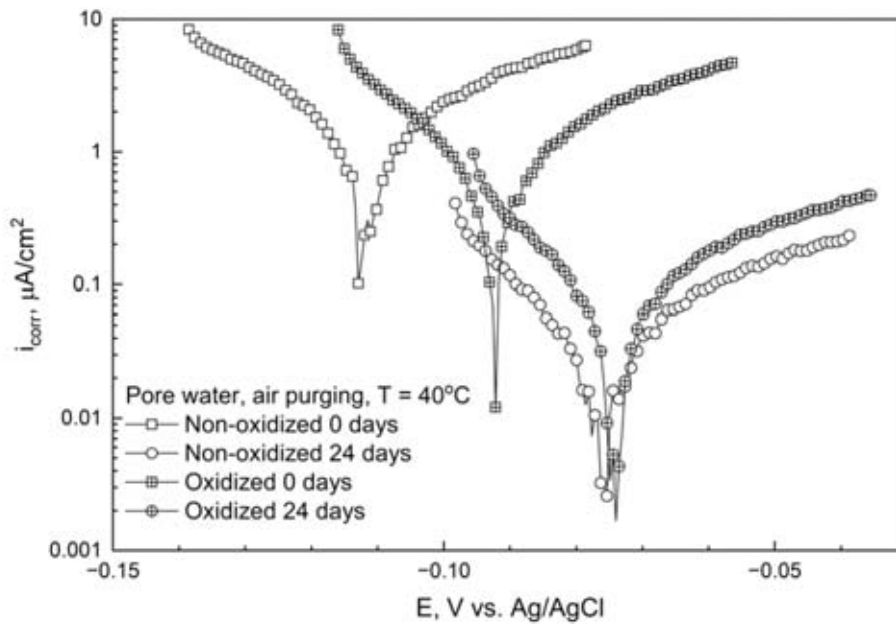
Figure 1. Example measurements in air-purged pore water at the beginning of the test and after 24 days.
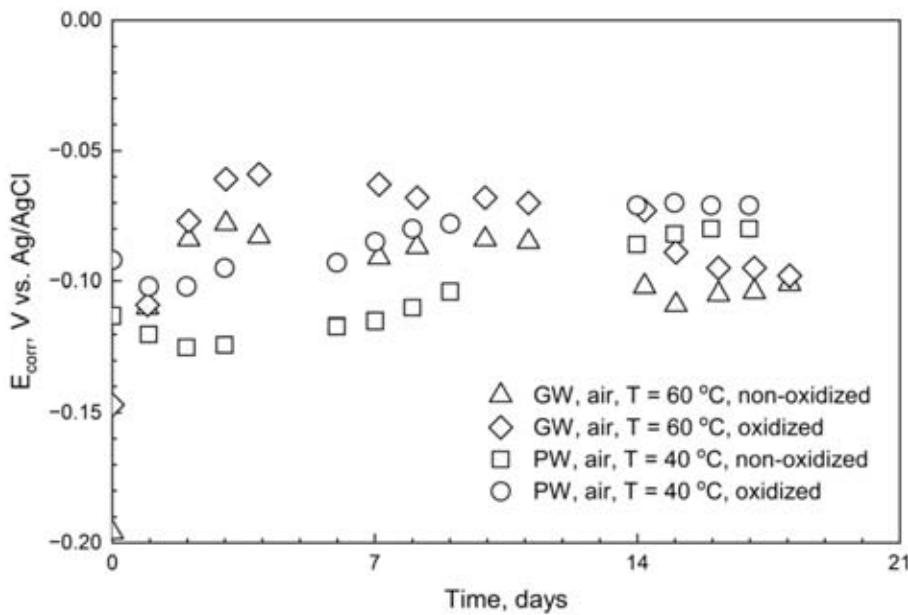
Figure 2. Evolution of the open circuit potential.

same environment. In our previous paper the corrosion rate was seen to decrease with time and in some cases the decrease followed a power law [14]. The formation of a corrosion product layer leading to passivity explains this phenomenon, but passivation is not always permanent. Figure 3 shows an example of a test with clear decrease in corrosion rate with time and Figure 4 shows an example where the effect of time and passivation is not clear. The first analysis method was to use confidence levels. As the number of replicate measurements in each test was small this was
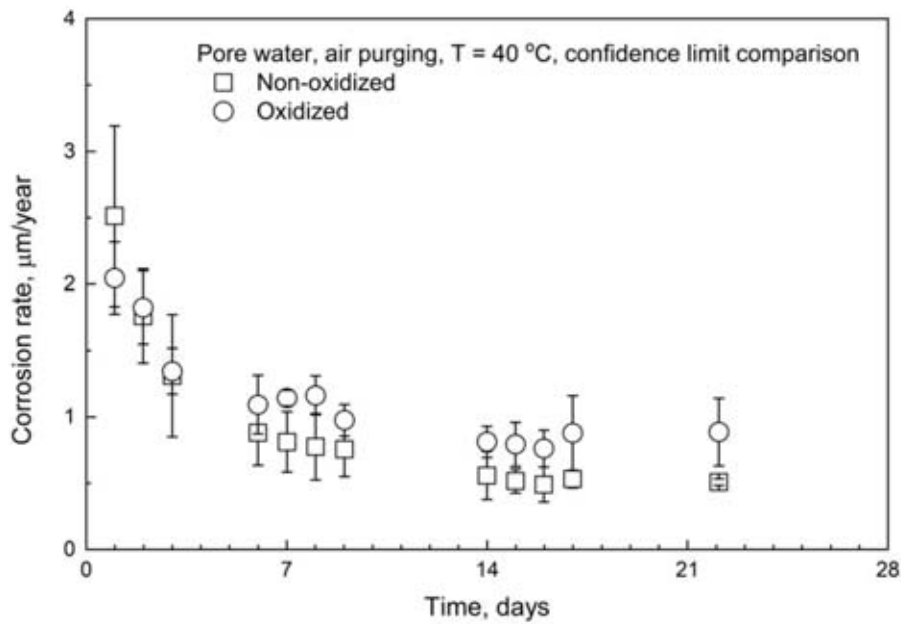
Figure 3. Comparison of measurements with clear decrease of corrosion rate with time using the 95% confidence limits.
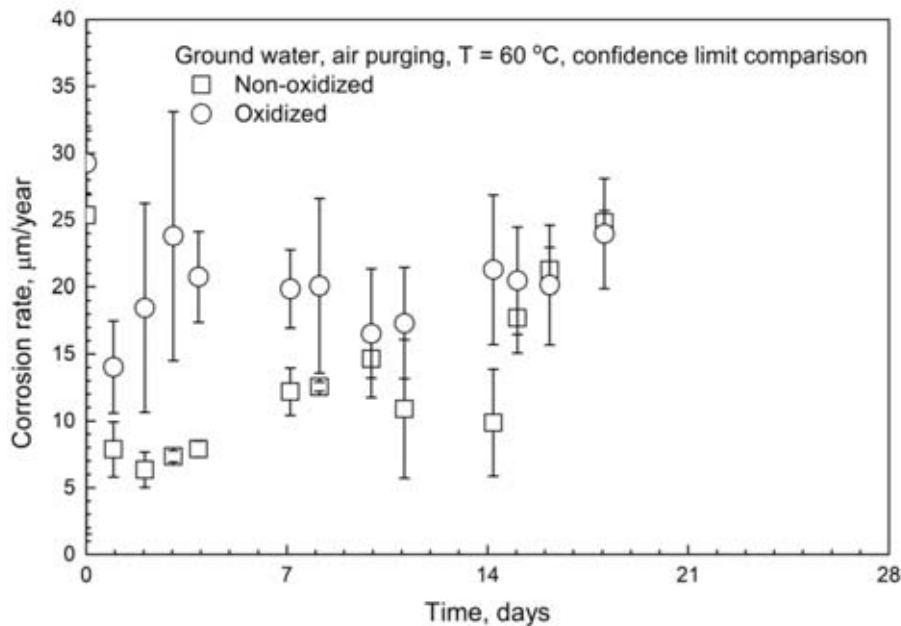
Figure 4. Comparison of measurements with random variation of corrosion rate with time using the 95% confidence limits.

taken into account using the t distribution. In this analysis the result is the average of the six replicate measurements (two samples, three measurements) and the confidence level standard deviation divided by the square root of measurements (6) multiplied by the Student t distribution factor 2.571 (N = 6, 95%), equation (1).

$$r = r(avg) \pm 2.571 \cdot s/\sqrt{6} \qquad (1)$$

If the confidence limits overlap, then the oxide film was concluded to have no effect. For example, comparison of the two samples in Figure 3 indicates that the oxide film can result in more rapid corrosion after about one week. Simple comparison of overlapping confidence limits as shown in Figures 3 and 4 proved to be ambiguous. The analysis is mainly based on visual evaluation and there is no definite method to analyze those cases where in some measurements the confidence limits overlap, and in some measurements not.

Another method to compare the oxidized and non-oxidized samples was to form a power law model using equation (2) and its double logarithmic plot (3).

$$r = A \cdot t^B \qquad (2)$$

$$\log(r) = \log(A) + B(\log(t)) \qquad (3)$$

In equations (2) and (3) r is corrosion rate in $\mu m\ a^{-1}$ and t is time in days. The factors of the power law A and B and their errors were determined by using linear regression to equation (3). This allowed calculation of minimum and maximum values for the corrosion rate using the power law. The model errors were estimated by calculating the minimum (4) and maximum (5) corrosion rates given by factors A and B and their errors α and β,

$$r_{min} = (A-\alpha) \cdot t^{(B-\beta)} \qquad (4)$$

$$r_{max} = (A+\alpha) \cdot t^{(B+\beta)} \qquad (5)$$

An example of the analysis using the power law method is shown in Figure 5. The model is calculated using equation (3) and the minimum and maximum values using equations (4) and (5) and these are presented as error band. In equation (2), the factor A value describes the initial corrosion rate and factor B value how corrosion rate changes with time. The more negative the value of factor B the more rapid the decrease in corrosion rate with time. The factor A alone is not a reliable indicator for corrosion rate as the time to reach a steady state can vary. Also, from the experimental point of view, the initial corrosion rate described by factor A can decrease quite

rapidly, which means that the initial state is no longer relevant after some tens of minutes. Therefore, the analysis was done by comparing the error band plots of oxidized and non-oxidized samples. If the error bands overlap, then the oxide film was concluded to not affect corrosion rate as shown in Figure 6.

The results of the effect of oxide film analysis using the power law are shown in Table 2, where the determined power law factor values and their errors are listed. The power law analysis was not applicable, if the factor A error was larger than the factor A value, factor B showed a positive value or factor B error was larger than factor B value. Those oxidized-non-oxidized sample pairs were not analysed using this method. If the factor A error is larger than the factor A value, the minimum corrosion rates calculated from equation (4) will get negative values. If the factor B has a positive value, then the corrosion rate calculated by the power law model will increase. If the factor B error is larger than the factor B value, the calculated maximum corrosion rates do not decrease with time resulting in very wide error band.

The corrosion rate was expected to decrease gradually with time. This was not seen in all tests, and typically caused by rapid passivation. Consequently, the resulting corrosion rate vs. time plot was linear from the beginning. In some cases, the current density started to increase after some time approaching a steady value. This was assumed to result from rapid passivation followed by slow depassivation. As noted in Table 2, 9 of the 16 measurements could not be analyzed using the power law method. However, also in these cases the calculated error bands did overlap indicating that the oxide film had no effect on corrosion rate.

As the power law was not applicable in all cases another analysis method was to consider the measured results as a replicate test series without the effect of time. If the first measurement point was clearly larger than the following ones it was discarded in the analysis. This analysis included the Excel t-Test: Two-Sample Assuming Unequal Variance combined with Box-and-Whisker plot. The null hypothesis of the analysis was that the
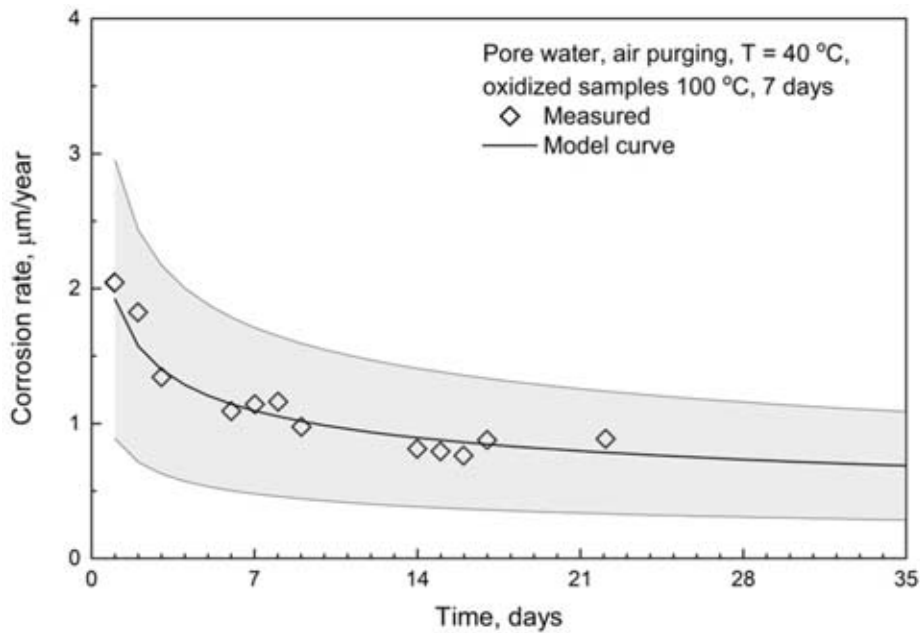
Figure 5. Example of corrosion rate model calculation using the power law method.
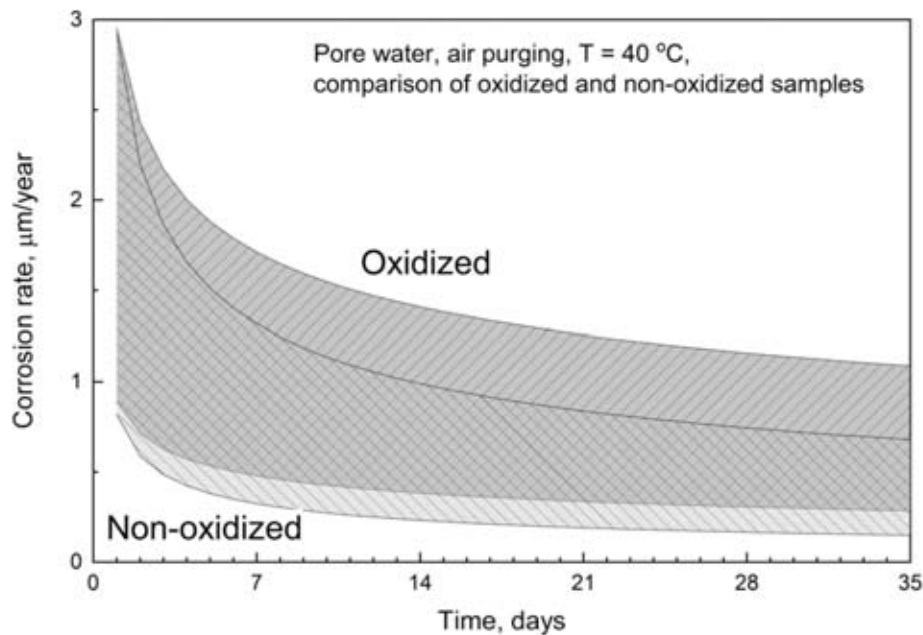
Figure 6. Analysis of the effect of oxide film using the power law method.

corrosion rates of oxidized and non-oxidized samples are the same. An example of this analysis method is shown in Figure 7. The data sets are ground water at T = 20°C with air purging and nitrogen purging. In the first column are the calculated corrosion rates in chronological order. The first measurements in the air-purged test were excluded because of the large difference of the non-oxidized sample. The box and whisker plots show that the medians and Q1 and Q3 quartile

Table 2. Power law modelling analysis results.

Water	Gas	T (°C)	Oxidation	A	B	Result
GW	Air	20	None	11.0 ± 1.09	-0.214 ± 0.036	Non-oxidized corrodes
GW	Air	20	100°C, 7 days	3.55 ± 1.03	-0.094 ± 0.014	faster
GW	Air	40	None	8.92 ± 1.23	-0.240 ± 0.084	Oxide film has no effect
GW	Air	40	100°C, 7 days	3.83 ± 1.06	-0.081 ± 0.027	
GW	Air	60	None	11.4 ± 1.17	-0.108 ± 0.071	Oxidized corrodes
GW	Air	60	100°C, 7 days	20.5 ± 1.07	-0.057 ± 0.030	faster
GW	Air	80	None	25.6 ± 1.13	-0.288 ± 0.056	Oxidized corrodes
GW	Air	80	100°C, 7 days	36.0 ± 1.05	-0.168 ± 0.024	faster
GW	N_2	20	None	2.77 ± 1.24	0.012 ± 0.085	Not applied
GW	N_2	20	100°C, 7 days	1.58 ± 1.19	0.127 ± 0.069	B > 0 for both
GW	N_2	40	None	5.22 ± 1.30	0.021 ± 0.097	Not applied
GW	N_2	40	100°C, 7 days	3.10 ± 1.11	0.180 ± 0.039	B > 0 for both
GW	N_2	60	None	15.8 ± 1.32	-0.100 ± 0.113	Not applied
GW	N_2	60	100°C, 7 days	16.6 ± 1.16	-0.186 ± 0.061	β > B for non-oxidized
GW	N_2	80	None	23.6 ± 1.06	0.184 ± 0.024	Not applied
GW	N_2	80	100°C, 7 days	25.2 ± 1.05	0.226 ± 0.021	B > 0 for both
PW	Air	20	None	2.11 ± 1.15	-0.311 ± 0.056	Not applied
PW	Air	20	100°C, 7 days	0.90 ± 1.27	-0.217 ± 0.098	α > A for oxidized
PW	Air	40	None	1.87 ± 1.05	-0.424 ± 0.021	Oxide film has no effect
PW	Air	40	100°C, 7 days	1.92 ± 1.03	-0.289 ± 0.013	
PW	Air	60	None	6.73 ± 1.11	-0.124 ± 0.043	Oxide film has no effect
PW	Air	60	100°C, 7 days	6.23 ± 1.10	-0.109 ± 0.036	
PW	Air	80	None	4.39 ± 1.17	-0.200 ± 0.076	Oxide film has no effect
PW	Air	80	100°C, 7 days	2.34 ± 1.15	-0.134 ± 0.065	
PW	N_2	20	None	0.47 ± 1.21	-0.202 ± 0.078	Not applied
PW	N_2	20	100°C, 7 days	1.10 ± 1.13	-0.163 ± 0.049	α > A for both
PW	N_2	40	None	1.98 ± 1.16	0.050 ± 0.059	Not applied
PW	N_2	40	100°C, 7 days	2.01 ± 1.17	-0.065 ± 0.062	B > 0 for non-oxidized
PW	N_2	60	None	5.16 ± 1.14	-0.101 ± 0.054	Not applied
PW	N_2	60	100°C, 7 days	5.15 ± 1.14	0.011 ± 0.055	B > 0 for oxidized
PW	N_2	80	None	7.61 ± 1.17	-0.041 ± 0.074	Not applied
PW	N_2	80	100°C, 7 days	4.62 ± 1.24	0.042 ± 0.100	B > 0 for oxidized
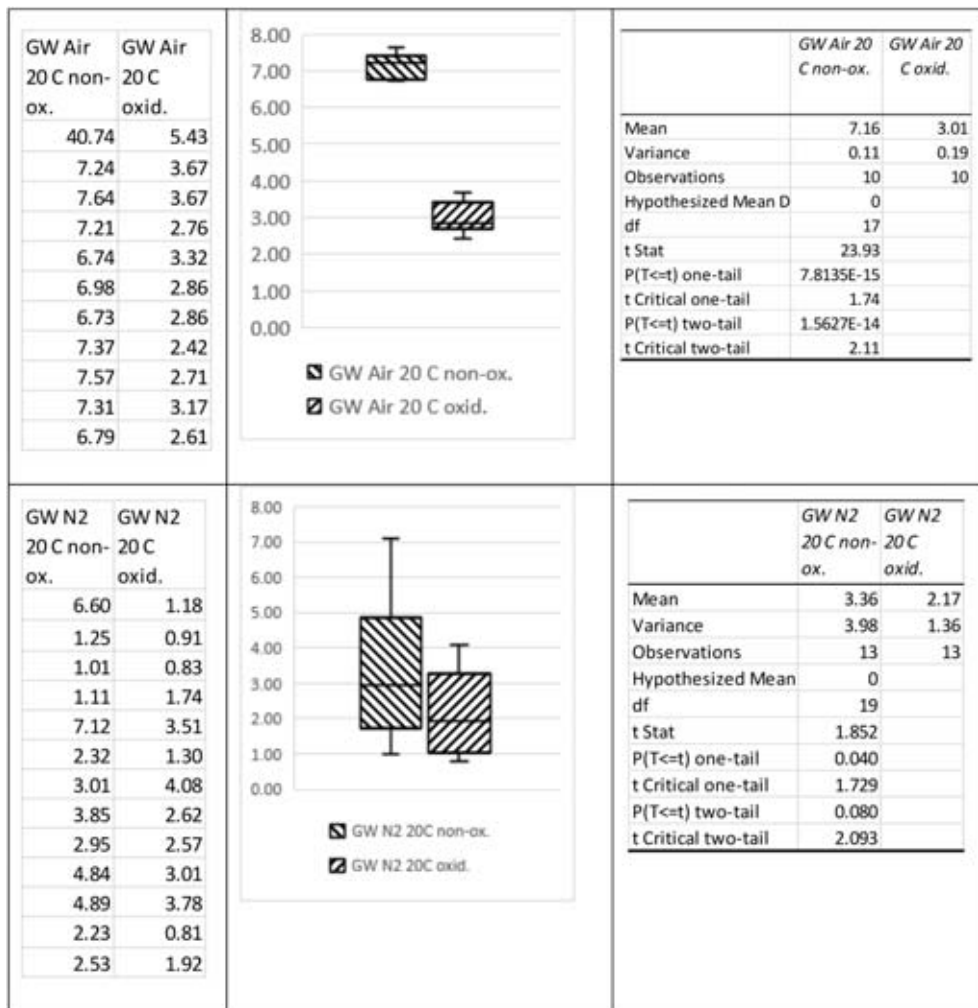
Figure 7. Evaluation of the oxide film effect using box-and-whisker plot and t-test.

boxes do not overlap for the air-purged samples, but they do overlap for the nitrogen-purged samples. The conclusion from the box and whisker plot is that in the air-purged system the corrosion rate of non-oxidized samples is higher, but in the nitrogen-purged system no significant difference is seen. The t-test result matrix using $\alpha = 0.05$ shows that the mean corrosion rate of non-oxidized samples is higher both in air and nitrogen-purged system. The test hypothesis was that the mean difference is zero; also corrosion rates are equal. For the air-oxidized samples the test value t Stat is 23.93 and two-tailed critical t value is 2.11. As $|23.93| > |2.11|$ the null hypothesis is rejected, and the corrosion rates differ. For the air-oxidized samples test value

t Stat = 1.852 and two-tailed critical t value is 2.093. As $|1.852| < |2.093|$ the null hypothesis is not rejected, and the corrosion rates do not differ.

The analysis using t-test was done by discarding the idea of decreasing corrosion rate and using the measured results as replicate tests. The corrosion rate was assumed to be constant with some random variation because of the rather short test time of 3-4 weeks. The analysis using t-test as shown in Figure 7 indicated that in most cases the oxide film had no significant effect on corrosion rate, Table 3.

Comparison of the two analysis methods shows that the conclusions are in most cases the same.

Table 3. t-test analysis results.

Water	Gas	T (^{o}C)	Oxidation	r_{mean} µm a^{-1}	t-test	Result
GW	Air	20	None	7.16	$\lvert 23.93 \rvert > \lvert 2.110 \rvert$	Non-oxidized corrodes
GW	Air	20	100°C, 7 days	3.01		faster
GW	Air	40	None	5.53	$\lvert 0.736 \rvert < \lvert 2.120 \rvert$	No difference
GW	Air	40	100°C, 7 days	4.82		
GW	Air	60	None	12.83	$\lvert -3.597 \rvert > \lvert 2.093 \rvert$	Oxidized corrodes faster
GW	Air	60	100°C, 7 days	20.17		
GW	Air	80	None	33.57	$\lvert -0.558 \rvert < \lvert 2.131 \rvert$	No difference
GW	Air	80	100°C, 7 days	39.65		
GW	N$_2$	20	None	3.36	$\lvert 1.852 \rvert < \lvert 2.093 \rvert$	No difference
GW	N$_2$	20	100°C, 7 days	2.17		
GW	N$_2$	40	None	6.85	$\lvert 1.637 \rvert < \lvert 2.131 \rvert$	No difference
GW	N$_2$	40	100°C, 7 days	4.37		
GW	N$_2$	60	None	18.54	$\lvert 0.696 \rvert < \lvert 2.110 \rvert$	No difference
GW	N$_2$	60	100°C, 7 days	14.87		
GW	N$_2$	80	None	29.3	$\lvert -0.869 \rvert < \lvert 2.086 \rvert$	No difference
GW	N$_2$	80	100°C, 7 days	34.1		
PW	Air	20	None	1.14	$\lvert 5.014 \rvert > \lvert 2.110 \rvert$	Non-oxidized corrodes
PW	Air	20	100°C, 7 days	0.61		faster
PW	Air	40	None	1.04	$\lvert -0.642 \rvert < \lvert 2.120 \rvert$	No difference
PW	Air	40	100°C, 7 days	1.20		
PW	Air	60	None	5.14	$\lvert -0.401 \rvert < \lvert 2.110 \rvert$	No difference
PW	Air	60	100°C, 7 days	4.98		
PW	Air	80	None	5.55	$\lvert 2.053 \rvert < \lvert 2.262 \rvert$	No difference
PW	Air	80	100°C, 7 days	2.71		
PW	N$_2$	20	None	0.49	$\lvert -3.965 \rvert > \lvert 2.110 \rvert$	Oxidized corrodes faster
PW	N$_2$	20	100°C, 7 days	1.06		
PW	N$_2$	40	None	2.38	$\lvert 0.718 \rvert < \lvert 2.086 \rvert$	No difference
PW	N$_2$	40	100°C, 7 days	2.09		
PW	N$_2$	60	None	5.05	$\lvert -0.608 \rvert < \lvert 2.086 \rvert$	No difference
PW	N$_2$	60	100°C, 7 days	5.60		
PW	N$_2$	80	None	6.49	$\lvert -0.711 \rvert < \lvert 2.064 \rvert$	No difference
PW	N$_2$	80	100°C, 7 days	7.26		

The cases with different results are following:

- Ground water, air-purging, T = 80°C: both methods show that oxidized samples corrode faster, but the difference in t-test is too small to be significant.

- Pore water, air-purging, T = 20°C: t-test shows that non-oxidized samples corrode faster, but in the power analysis the initial corrosion rate error was too big for the oxidized samples. The power law model shows that the corrosion rate of the non-oxidized samples is larger.

- Pore water, nitrogen-purging, T = 20°C: t-test shows that oxidized samples corrode faster, but in the power analysis the initial corrosion rate error was too big for both samples. The power law model shows that the corrosion rate of the oxidized samples is larger.

A summary of the two analyses is given in Table 4 as ratio of the corrosion rates, oxidized/non-oxidized. The corrosion rates for the power law method are calculated using the model parameters in Table 2 without their errors and 21 days test time. The corrosion rates for t-test method are the values shown in Table 3. As shown in Table 4, in most cases the corrosion rate of the oxidized samples was lower; in 10 cases of 16 when using power law corrosion rates and in 9 cases when using t-test corrosion rates. There are no clear trends where the corrosion rates of oxidized samples are higher, except that they are more common at T = 60°C and T = 80°C than at lower temperatures.

The test waters were under constant purging with air or nitrogen, and the concentration of dissolved oxygen in air-purged waters was 6-7 ppm and in nitrogen-purged waters approximately 1 ppm. The maximum concentration of dissolved oxygen in modelling of copper corrosion has been taken as 8 ppm giving corrosion current densities in the order of 0.01 μA cm^{-2} in system where mass transport is limited by bentonite clay [4]. When comparing the tests in air-purged and nitrogen-purged waters and assuming oxygen corrosion in a diffusion-controlled system, the corrosion rate in nitrogen-purged system should be approximately 15% of that in air-purged system. The results in Table 3 indicate that the corrosion rates of non-oxidized samples in nitrogen-purged systems are approximately 90% of those in air-purged systems. The corrosion rates of oxidized samples in nitrogen-purged systems are approximately 80% of those in air-purged systems. This indicates that copper corrosion has not been under diffusion control of oxygen.

The corrosion rate of copper decreases with increasing pH. The corrosion rates in Table 3 show that the corrosion rates of non-oxidized samples in pH = 10 pore water are 20% of those in pH = 8 ground water, and those of oxidized samples 10%. The pH has strong influence on passivation as stated in [11]. In alkaline solutions copper corrosion results in the formation of Cu_2O with outer layer consisting of CuO and $Cu(OH)_2$ [11, 15]. In simulated tap water with low amount of dissolved solids Feng *et al.* found that from

Table 4. The effect of oxide film calculated by dividing the corrosion rate of oxidized sample with the corrosion rate of non-oxidized sample.

Method	Water	Gas	T = 20°C	T = 40°C	T = 60°C	T = 80°C
Power law	GW	Air	0.46	0.69	2.10	2.01
Power law	GW	N_2	0.81	0.96	0.81	1.14
Power law	PW	Air	0.57	1.55	0.97	0.65
Power law	PW	N_2	2.64	0.71	1.40	0.78
t-test	GW	Air	0.42	0.87	1.57	1.18
t-test	GW	N_2	0.65	0.64	0.80	1.16
t-test	PW	Air	0.54	1.15	0.97	0.49
t-test	PW	N_2	2.16	0.88	1.11	1.12

pH 6 to pH 9, the anodic dissolution process was controlled by diffusion in Cu_2O film [16]. At pH 10, a dense Cu_2O film was formed, resulting in spontaneous passivation [16]. The corrosion current densities in [16] were in the order of 1-2 μA cm^{-2} at the pH range 6-11, with a minimum of 0.5 μA cm^{-2} at about pH = 10, which is approximately 50-75% decrease. Our measurements showed 80-90% decrease of corrosion rate in pore water when compared with ground water.

The effect of temperature was estimated by calculating the activation energies according to Arrhenius law using the corrosion rates shown in Table 3. The results are shown in Table 5. The activation energies are in the order of 20-40 kJ mol^{-1} indicating that either a chemical or electrochemical process is rate-determining. For example, in bicarbonate solutions with formation of a porous reaction product layer corrosion has been controlled by mass transfer with activation energies in the order of ~10 kJ mol^{-1} [17]. In ground water the activation energy of a non-oxidized sample is lower than that of an oxidized sample. This can be due to the protective effect of the air-formed oxide; even the results in Tables 2 and 3 indicate that the oxide film has no effect. In pore water the activation energies are approximately the same for oxidized and non-oxidized samples indicating that the air-formed oxide film does not affect corrosion. It is likely that the passive film formed during immersion gives better protection than the air-formed oxide film.

CONCLUSIONS

The LPR monitoring provided instantaneous corrosion rates in different conditions resembling the post-closure repository environment during the oxic period and during the period when the underground environment changes to oxygen deficient. The general corrosion rate ranges from less than 1 μm/year to 40 μm a^{-1}, highest in air-purged ground water and lowest in nitrogen-purged pore water.

The concentration of dissolved oxygen was in air-purged waters, 6-7 ppm, and in nitrogen-purged waters approximately 1 ppm. Assuming oxygen corrosion in a diffusion-controlled system, the corrosion rate in nitrogen-purged system should be approximately 15% of that in air-purged system. In our measurements the difference between air-purged and nitrogen purged systems was only 10-20% indicating that corrosion was not controlled by oxygen reduction reaction.

The main differences in the water type are pH and total dissolved solids. Comparison of corrosion rates between pH = 8 ground water and pH = 10 pore water shows that the corrosion rates in pore water are 80% lower for oxidized samples and 90% for non-oxidized samples. This was caused by passivation during immersion.

Activation energy calculations showed that corrosion is not controlled by mass transfer. This supports the conclusion between air-purged and nitrogen purged tests. The differences in activation energies were so small that the air-formed oxide

Table 5. Activation energies of oxidized and non-oxidized samples.

Water	Gas	Oxidation	E_A (kJ mol^{-1})
GW	Air	None	22.9 ± 9.7
GW	Air	100°C, 7 days	39.2 ± 6.0
GW	N_2	None	32.3 ± 2.6
GW	N_2	100°C, 7 days	40.7 ± 3.8
PW	Air	None	27.1 ± 10.1
PW	Air	100°C, 7 days	26.0 ± 11.5
PW	N_2	None	37.2 ± 7.7
PW	N_2	100°C, 7 days	29.2 ± 3.6

film does not have an effect on corrosion mechanism.

Three different methods were used to determine whether an air-formed oxide film can result in higher corrosion rate of copper in synthetic natural waters. Comparison of confidence limits was not useful as the relative corrosion rates of oxidized and non-oxidized samples can change with time. The use of power law models takes into account the variation of corrosion rates with time, but this method is applicable only if the corrosion rate decreases gradually with time. The use of box-and-whisker plots combined with two-sample t-test and discarding the time effect was applicable for all tests.

Although the impact of air-formed oxide films varied, generally they had no significant impact on corrosion. The air-formed oxide film does not give significant corrosion protection, and the passive film formed during immersion is more efficient. On the other hand, the air-formed oxide film generally does not result in higher corrosion rates.

ACKNOWLEDGEMENTS

CONFLICT OF INTEREST STATEMENT

The authors declare no conflict of interest. The funders had no role in the design of the study; in the collection, analyses, or interpretation of data; in the writing of the manuscript, or in the decision to publish the results.

REFERENCES

1. Posiva, Oy. 2017, Safety Case Plan for the Operating Licence Application. Report POSIVA 2017-02, Posiva Oy, Eurajoki, 152.
2. Posiva, Oy. and Svensk Kärnbränslehantering, A. B. 2017, Safety functions, performance targets and technical design requirements for a KBS-3V repository. Report POSIVA-SKB 2017-01, Posiva, Oy. and SKB., 120 p.
3. Raiko, H., Pastina, B., Jalonen, T., Nolvi, L., Pitkänen, J. and Salonen, T. 2012, Canister Production Line 2012. Report POSIVA 2012-16, Posiva, Oy, Eurajoki, 174 p.
4. King, F., Lilja, C., Pedersen, K., Pitkänen, P. and Vähänen, M. 2012, An Update of the State-of-the-art Report on the Corrosion of Copper Under Expected Conditions in a Deep Geologic Repository. Report Posiva 2011-01, Posiva, Oy., Eurajoki, 246 p.
5. Nolvi, L. 2009. Manufacture of Disposal Canisters. Report Posiva 2009-03, Posiva Oy, Eurajoki, 76 p.
6. King, F. and Kolář, M. 2018, Corrosion, 75, 309.
7. Vazquez, M. V., de Sanchez, S. R, Calvo, E. J. and Schiffrin, D. J. 1994, J. Electroanal. Chem., 374, 189.
8. King, F., Quinn, M. J. and Litke, C. D. 1995, J. Electroanal. Chem., 385, 45.
9. Vukmirovic, M. B., Vasiljevic, N., Dimitrov, N. and Sieradzki, K. 2003, J. Electrochem. Soc., 150, B10.
10. King, F., Kolář, M. and Maak, P. 2008, J. Nuc. Mat., 379, 133.
11. King, F. 2002, Corrosion of copper in alkaline chloride environments. Technical Report TR-02-25, SKB, Stockholm, 77 p.
12. Huttunen-Saarivirta, E., Rajala, P. and Carpén, L. I. 2016, El. Acta, 203, 350.
13. Vikman, M., Matusewicz, M., Sohlberg, E., Miettinen, H., Järvinen, J., Itälä, A., Rajala, P., Raulio, M., Itävaara, M., Muurinen, A., Tiljander, M. and Olin, M. 2018, Long-term experiment with compacted bentonite. VTT Technology, Report No. 332. VTT Technical Research Centre of Finland, Espoo, 84 p.
14. Aromaa, J., Khalid, M. K., Aji, A. T. and Lundström, M. 2021. Curr. Top. Electrochem., 23, 81.
15. Babic, R., Metikos-Hukovic, M. and Jukic, A. 2001. J. Electrochem. Soc., 148, B146.
16. Feng, Y., Siow, K-S., Teo, W-K., Tan, K-L. and Hsieh, A-K. 1997, Corrosion, 53, 389.
17. Drogowska, M., Brossard, L. and Ménard, H. 1993. J. Electrochem. Soc., 140, 1247.